Applied Surface Science 535 (2021) 147621

Contents lists available at ScienceDirect

Applied Surface Science

journal homepage: www.elsevier.com/locate/apsusc

Tantalum coating inhibits Ni-migration from titanium out-diffusion in NiTi shape memory biomedical alloy

K. McNamara[a,b,*], S. Beloshapkin[a], K.M. Hossain[c], M.S. Dhoubhadel[c], S.A.M Tofail[a,b,*]

[a] Bernal Institute, University of Limerick, Limerick, Ireland
[b] Department of Physics, University of Limerick, Limerick, Ireland
[c] Amethyst Research, Inc., 123 Case Circle, Ardmore, OK 73401, USA

ARTICLE INFO

Keywords:
NiTi
Shape memory alloy
Biomedical alloy
Minimally invasive surgical devices
Tantalum oxide coating
Ti migration
Ni-leaching
XPS
RBS

ABSTRACT

Despite the presence of over 56% Ni by weight, equiatomic NiTi is generally considered biocompatible as it naturally oxidises to form a surface oxide mainly composed of biocompatible oxides of titanium (TiO_x). This layer is formed by an oxidation mechanism that promotes out-diffusion of Ti leaving a Ti-depleted, Ni rich subsurface. The long-term *in vivo* stability of the naturally grown TiO_x layer has been a concern as Ni can leach out through this thin, defective layer. The leaching of nickel (Ni) is thus a continuing threat to the alloy's otherwise outstanding biocompatibility. We have found that a layer of reactively sputtered tantalum (Ta) oxide on the bulk NiTi restricts Ti-out-migration through a biocompatible Ti/Ta inter-diffusion layer that provides a larger barrier against Ni leaching. We have investigated this inter-diffusion as a function of sputtering process parameters and post processing treatments. Surface and interface analytical techniques such as X-ray photoelectron spectroscopy, scanning electron microscopy, energy dispersive X-ray spectroscopy, cross sectional transmission electron microscopy and non-destructive ion beam analysis techniques such as Rutherford backscattering spectrometry and particle induced X-ray emission were used to evaluate the nature of this inter-diffusion layer which can improve long-term biocompatibility of NiTi.

1. Introduction

Equiatomic NiTi, commonly referred to as Nitinol, is used in many medical device applications due to its unique properties such as shape memory and superelasticity and a biocompatible surface [1–6]. Shape memory effect allows the material to return to its original shape upon heating or cooling. Superelasticity allows the alloy to deform beyond yield point on mechanical loading that can be reversed during unloading for a few million cycles. These distinctive properties have resulted in the use of NiTi in various applications particularly biomedical devices such as orthodontic wire guides, braces, self-expandable vascular stents, urinary stents and catheters [6,7].

Due to the high concentration of Ni in NiTi there has been concerns regarding its use in biomedical devices, especially for long-term use as implants [8–10]. NiTi naturally oxidises to form a surface oxide layer TiOx, which is mainly composed of titanium dioxide (TiO_2). This TiO_2 layer provides the NiTi alloy with its biocompatibility and allows for its use in biomedical applications. This oxide layer forms from oxygen in the atmosphere that reacts with titanium on the surface of the alloy. This thin layer is expected to act as a barrier against the release of undesirable Ni^{2+} ions into the body [10–17].

Atomistic simulation has shown that the oxidation mechanism involves an outward diffusion of Ti to combine with oxygen by breaking the Ni-Ti bond at the surface [17]. During the adsorption of oxygen on the surface of NiTi, Ti is pulled out from the bulk to bond with the oxygen in the atmosphere. This out-migration of Ti can cause a depletion of Ti at the subsurface thus leaving behind a Ni-rich layer [18,19]. The out-migration and the resulting depletion of Ti at the oxide/NiTi interface has been observed in cross sectional transmission electron microscopy. A Ni-rich subsurface so formed can prompt Ni-leaching through the otherwise biocompatible but thin (~5–10 nm) [20] and defective [9,21] oxide layer.

Obviously, this raises concerns regarding the stability of this naturally grown TiO_x layer on NiTi, as a possible breakdown of this layer within the body, for example by body fluids, may cause a release of toxic Ni^{2+} ions [22–25] and compromise the alloys biocompatibility [19]. This problem is well-known in the biomedical device manufacturing industry and various methods such as anodic oxidation [26–31], thermal oxidation [32–37], electropolishing [38], and coating techniques [39–47] have been used to improve the stability and quality

* Corresponding authors at: Bernal Institute, University of Limerick, Limerick, Ireland.
E-mail addresses: Karrina.McNamara@ul.ie (K. McNamara), Tofail.Syed@ul.ie (S.A.M. Tofail).

https://doi.org/10.1016/j.apsusc.2020.147621
Received 28 February 2020; Received in revised form 10 August 2020; Accepted 14 August 2020
Available online 29 August 2020

of this TiO_x layer.

One such method of improving the biocompatibility and the stability of NiTi is to deposit a more stable and better-adherent film on the surface of NiTi. In this study, we sputter coat NiTi with a tantalum oxide film. Both tantalum and tantalum oxide are known to be biocompatible and unaffected by body fluids [48–53]. The deposition of tantalum and tantalum oxide films has received some attention in literature [50–74]. Tantalum oxide films can be deposited either chemically using for example electrodeposition, or physically using sputter deposition. Both methods offer many advantages, but we chose sputtering as it offers an ease of deposition and better control of the thickness of the film. Reactive sputter deposition (RSD) of tantalum and tantalum oxide films has been carried out on a number of substrates [52–55,73,74] however deposition of these films on NiTi has been limited. The effect of RSD and post-deposition treatments on the interface between NiTi surface and Ta-oxide coating has not been reported so far.

In this work, we investigate the effect deposition and post-processing parameters have on the films surface and interfacial chemistry, morphology and structure. We report that a layer of reactively sputtered tantalum (Ta) oxide on the bulk NiTi restricts Ti-out-migration and creates a biocompatible Ti/Ta inter-diffusion layer that can possibly provide a larger barrier against Ni leaching. Supplemental Information (SI) provides an elaborate list of literature on anodization of NiTi, oxidisation of NiTi, electropolishing of NiTi, coatings on NiTi, biocompatibility of Ta and sputter deposition of Ta and Ta oxide films.

2. Materials and methods

A cold rolled, slightly Ti-rich (Ti–55 wt% Ni) NiTi sheet (American Elements, USA) was cut into several 20 × 10 × 1 mm plates. Each sample was mechanically polished using a Phoenix 4000 sample preparation system to obtain an identical surface finish of 4000 grit size. Tantalum films were deposited on NiTi substrates using radio frequency (rf) magnetron sputtering using a load-locked ATC Orion Deposition System (AJA International Inc., USA). For reactive sputtering of Ta-oxide, oxygen was introduced into the chamber as a mixture with argon. The total pressure in the chamber was kept at 0.4 Pa with an argon to oxygen ratio of 90 to 10 (90/10) with a target to substrate distance of 15 cm. These parameters were chosen after optimising the sputtering conditions to avoid oxidation of the Ta target during reactive sputtering with oxygen. The thickness of the films was measured using an in-line quartz crystal microbalance.

NiTi substrates were heated to 80 °C to aid with the deposition process. The deposition power was kept constant at 100 W (4.93 W/cm^2) while the deposition time (thickness) was varied. The tantalum oxide deposition was carried out for 20, 50 and 90 min. In another set of samples, we applied to the substrate a negative bias of −100 V during the deposition process, with all other parameters remaining the same. All films under investigation were then annealed at 800 °C either in air or in vacuum. 800 °C was chosen as from X-ray diffraction (XRD) data it could be seen that the tantalum oxide films were not fully crystalline below 800 °C and above 800 °C cracking of the tantalum oxide film occurred.

Table 1 provides a summary of the deposition parameters and post-processing treatments of the samples investigated in the present study.

The morphology and elemental composition of the Ta-oxide films were investigated using a Hitachi SU-70 field emission scanning electron microscope (FE-SEM) and an Oxford Instruments energy dispersive X-ray spectroscopy (EDX) probe which were operated at 20 kV for the experiment. FEI-FIB 200 workstation was used to prepare the sample for TEM analysis. A JEOL JEM-2100F field emission transmission electron microscope (FE-TEM) operated at 200 kV using the dark field detector was used to analyse the interface between the film and substrate. The approximate thickness of the samples was 0.1–0.2 μm. Energy dispersive X-ray spectroscopy (EDX) was carried out using an EDAX Genesis EDX detector. The spectral lines used for construction of the EDX data and maps were O (K), Ni (K), Ta (L), Ti (K) and Pt (L). A Kratos AXIS 165 X-ray photoelectron spectrometer (XPS) was used to investigate the surface chemistry and oxidation states of the films. A beam voltage of 15 kV and beam current of 10 mA were the operating conditions used. The binding energies were determined by using C 1s peak at 284.8 eV as the charge reference. A Shirely type background was used to construct and fit the synthetic peaks in the narrow region and the synthetic peaks were a mixed Gaussian-Lorenzian type. The spin orbit split applied to the peaks was 0.75. Various oxidation states of Ta have been assigned based on the discussion given in McNamara et al [53,55]. As received NiTi alloy sample and the deposited TaOx thin films were analysed by a simultaneous Rutherford backscattering spectrometry (RBS) and particle induced X-ray emission (PIXE) spectrometry. Rutherford backscattering spectrometry (RBS) is a non-destructive analytical technique for materials characterization where the energy spectrum of elastically backscattered ions is used to determine the film's parameters, i.e., composition and thickness. The energy of a backscattered ion is determined by a standard solid-state, surface-barrier detector, which is integrated with standard pulse processing modules to yield a histogram of the backscattering events for measuring the thickness of the oxide layers, diffusion profile, as well as the composition and the films. Spectral simulation using a standard computer code, SIMNRA, was used to achieve the best fit to the experimental spectra to determine parameters such as composition and the thickness from the parameters used in the simulated spectra. Besides elastic scattering during RBS, inelastic scattering between an energetic ion and a target atom occurred and lead to inner shell ionization with the subsequent emission of an x-ray. The energy of the x-ray, which is characteristic of the excited atom, is detected by a solid-state Si (Li) PIXE detector. During simultaneous data collection, RBS and PIXE detectors were placed at 160 and 135 scattering angles respectively. A beam of 1.5 MeV $^4He^+$ was used for ion beam analysis using the 2.5MV van de Graaff accelerator facility at Amethyst Research, Inc.

Table 1
Summary of the thickness, deposition parameters and post-processing treatments of Ta oxide films deposited onto NiTi plates.

Sample ID	Film Thickness (nm)	Deposition Parameters Bias (V)	Post Processing Treatment	
			Annealing Temperature (°C)	Annealing Environment
Sample 1	640	–	–	–
Sample 2	665	−100 V	–	–
Sample 3	635	–	800 °C	Air
Sample 4	662	−100 V	800 °C	Air
Sample 5	700	–	800 °C	Vacuum
Sample 6	670	−100 V	800 °C	Vacuum
Sample 7 (NiTi)	–	–	–	–

3. Results and discussion

3.1. SEM morphology and EDX chemistry

Scanning electron micrographs in Fig. 1 show the morphology of the reactively sputtered tantalum oxide films especially the change of the morphology with respect to annealing environment (i.e. in air or in vacuum) and whether a negative bias voltage has been used during sputtering. The morphology of the as deposited tantalum oxide films appears to be smooth and featureless, amorphous irrespective of the bias (Fig. 1(a) and (b)). Annealing of the RSD films at 800 °C in air and in vacuum, expectedly, made these films more crystalline (Fig. 1(c)–(f)). Fig. 1(f) shows a more crystalline morphology. Some films, such as the film deposited with a bias and annealed in air (Fig. 1(d)) and the film deposited without bias and annealed in vacuum

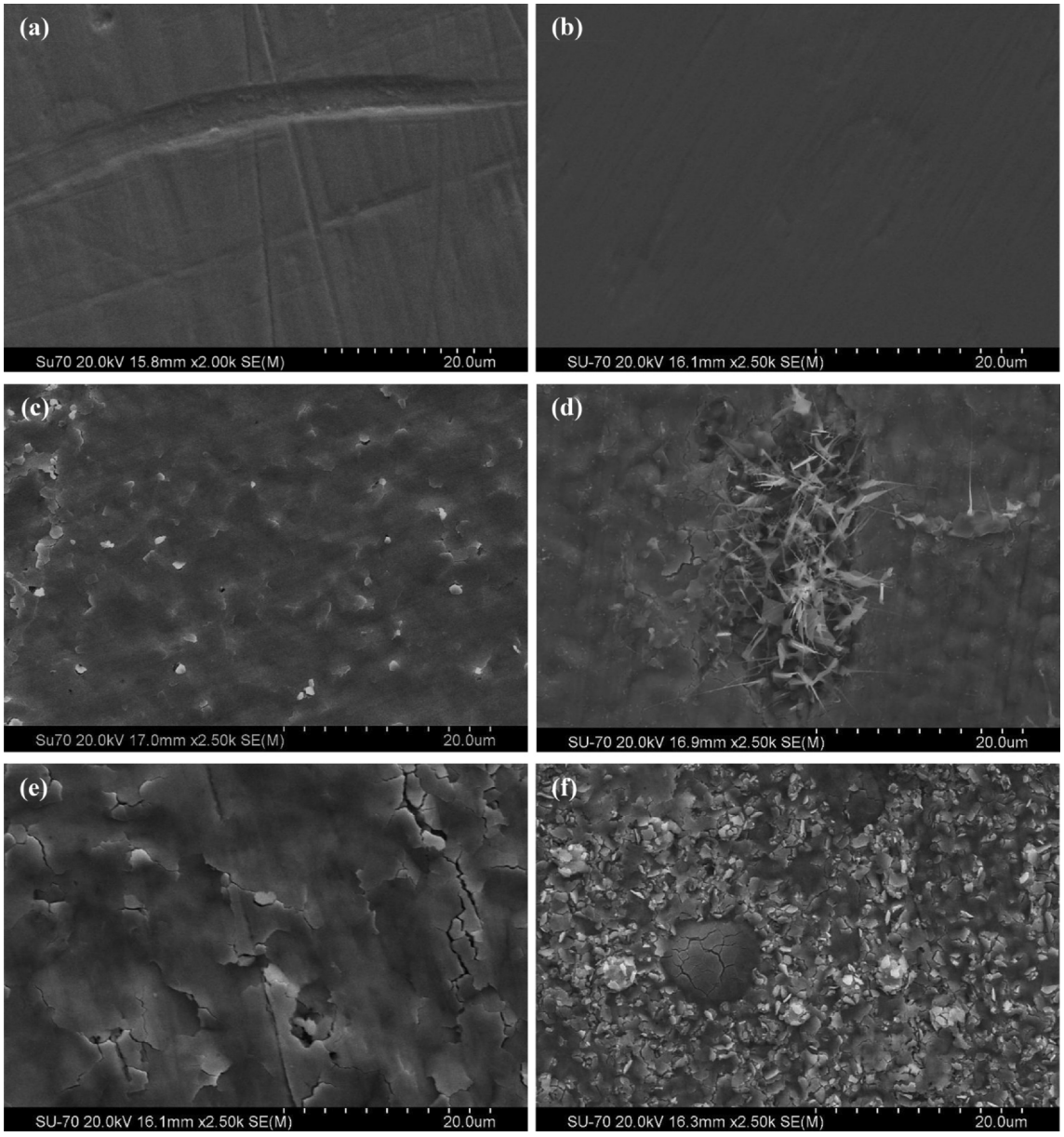

Fig. 1. SEM micrographs comparing the morphology tantalum oxide films deposited onto NiTi substrates and subjected to different conditions. Figure (a) as deposited without a bias, (b) as deposited with a bias, (c) annealed at 800 °C in air without bias, (d) annealed at 800 °C in air with bias, (e) annealed at 800 °C in vacuum without bias and (f) annealed at 800 °C in vacuum with bias.

(Fig. 1(e)) showed cracks. Thus, both deposition and post-processing parameters have impact on the morphology, crystallinity and residual stress in the films. The changing morphology of the Ta-oxide films could affect the biocompatibility of the device in the human body. The surface morphology is linked with roughness and if the roughness is too low or too high this could affect the adherence of the device in the body. For implantation in the body we would need to address these issues to find the ideal film thickness, surface roughness and morphology to allow the Ta-coated NiTi device to retain its shape memory and elastic properties as well as it's biocompatibility.

The processing parameters can have an important influence on the surface and interface chemistry as is seen from the Energy dispersive X-ray spectroscopy (EDX) analysis in Figs. 2 and 3. Fig. 2(a) is a SEM micrograph which shows the outmigration of Ti through the Ta-oxide film. Fig. 2(b) displays the EDX analysis of the selected areas, which shows that this in mainly Ti (52 wt%) and O (46 wt%) and a small amount of Ta (2%) was also detected. This is likely from the surrounding area as EDX generally analyses a larger area than is selected. Fig. 3 shows the EDX analysis of the Ta-oxide films deposited onto NiTi under various parameters. The purpose of this graph is to compare the bulk chemistry of the films and how it varies with different pre and post processing parameters. While the general chemistry of these films comprises a mixture between tantalum, titanium and nickel in as deposited films with or without a bias during deposition. From the data from Fig. 3, there is a significant difference between the Ta to Ti ratio between films deposited with bias (19:1) and deposited without bias (9:1). The application of a negative bias during deposition of Ta-oxide films has resulted in a denser and slightly thicker (665 nm) film than the as deposited Ta- oxide film which has a thickness of 640 nm, Table 1. Due to the denser and thicker Ta-oxide film, the EDX would not detect as much titanium and therefore explain the concentration difference between the films. Despite the use of oxygen in reactive sputtering, we did not detect much oxygen, only 17–18 wt%, in the as deposited films by EDX. This is due to the 90:10 ratio of Argon to Oxygen

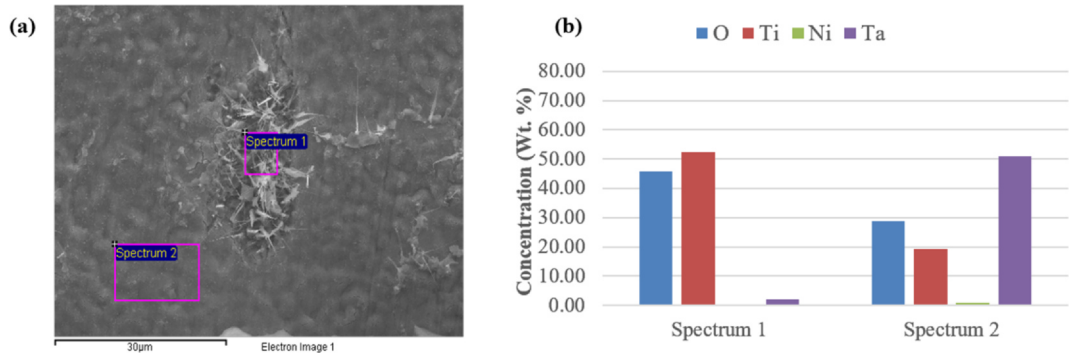

Fig. 2. (a) Selected area EDX of tantalum oxide films deposited onto NiTi without a bias and annealed at 800 °C in vacuum and (b) bar graph showing the concentrations of titanium, nickel, tantalum and oxygen in the selected areas.

that is used during the deposition process. From the data in Fig. 3, it can be seen that annealing has maintained a similar trend of Ta to Ti ratio between films deposited with bias (6:1 in air and 4:1 in vacuum) and without bias (1:1 in air and 1:1 in vacuum).

The application of a bias during deposition generally resulted in a higher Ta to Ti ratio, a trend that is maintained during both air and vacuum annealing. The application of a negative bias has possibly allowed for the formation of a denser tantalum oxide film.

Annealing in air and in vacuum, which also introduces oxygen gives rise to a complex scenario of oxidation kinetics between the presence of oxygen in air, base oxygen in vacuum, the presence of Ta and Ni and the application of a bias. Ti has a significantly higher affinity for oxygen than Ni [75] which allows Ti in NiTi to be pulled outward leading to an enrichment of TiO_2 in the outermost layer. This is not the case for the Ta–Ti system where the oxygen affinity is comparable [76] but with Ti having a slightly higher affinity. The gas phase oxidation kinetics of Ta–Ti alloys between 800 and 1400 °C showed a complicated situation due to the simultaneous presence of Ta and oxygen with Ti. While oxygen acts as a stabilizer of α-phase of Ti, tantalum stabilises the β-phase of Ti. Tantalum is also found to have decreased the diffusivity of Ti and the solubility of oxygen. As a result, the relation between composition and minimum oxidation rate depends on the temperature and the atmosphere [77]. Together, and more interestingly, the RSD of tantalum oxide resulted in a suppressed amount of Ni within the EDX probe area. This is significant when we consider that annealing at a far less harsh condition (e.g. 450 °C for 30 min) has previously been reported to have resulted in a strong presence of Ni at the surface [10,33]. The presence of tantalum thus has contributed to the suppression of Ni within the outer surface but not only creating a thicker over-layer of tantalum but also suppressing the out-diffusion of titanium. Annealing in vacuum with a negative bias seems to provide the best possible combination of desirable chemistry, crystallinity and lack of cracking. According to theory applying a negative bias to the substrate during the deposition process can modify some of the deposited films properties such as resistivity, hardness, residual stress and optical resistivity. Some advantages of applying a negative bias include higher film density and improved adhesion [78].

3.2. Surface and interface chemistry by XPS and RBS

X-ray photoelectron spectroscopy was used to study the surface and interface chemistry of as deposited and annealed tantalum oxide films described in the previous section. As can be seen from Fig. 4, there is no significant difference in the surface concentrations in these films. The atomic concentration of tantalum, oxygen and carbon present on the surface do not vary significantly. We do not observe the presence of Ti at the surface of the unbiased and biased as-sputtered films. This is due to the penetration depth of the soft X-rays used for XPS, the analysis depth is between 1 and 10 nm. From Fig. 4, the ratio of Ta to Ti is approximately 6:1 for the samples annealed in air and 7:1 for the sample annealed in air with a bias. The application of a bias produces a more-dense Ta-oxide film and Ti out-migration through the Ta-oxide film is not as prominent. The sample deposited with a bias generally produces a thick Ta-oxide film also. The ratio of Ta to Ti for the films annealed in vacuum is approximately 0.7:1 for the Ta-oxide film annealed in vacuum. The Ta to Ti ratio for the samples annealed in

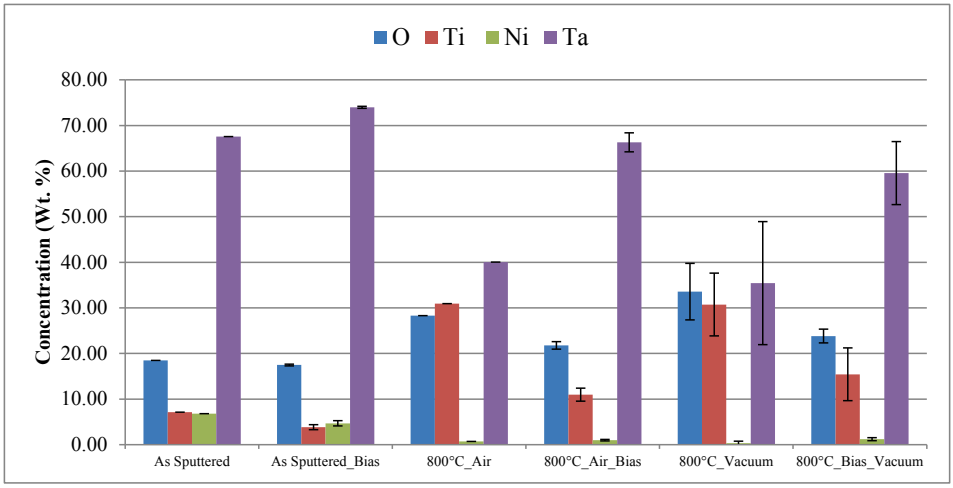

Fig. 3. Graph showing the average concentration of titanium, nickel, tantalum and oxygen obtained by Energy dispersive X-ray spectroscopy. EDX was used to analyse the bulk chemistry of the tantalum oxide films deposited with a bias of −100 V and compared to the tantalum oxide films deposited without a bias.

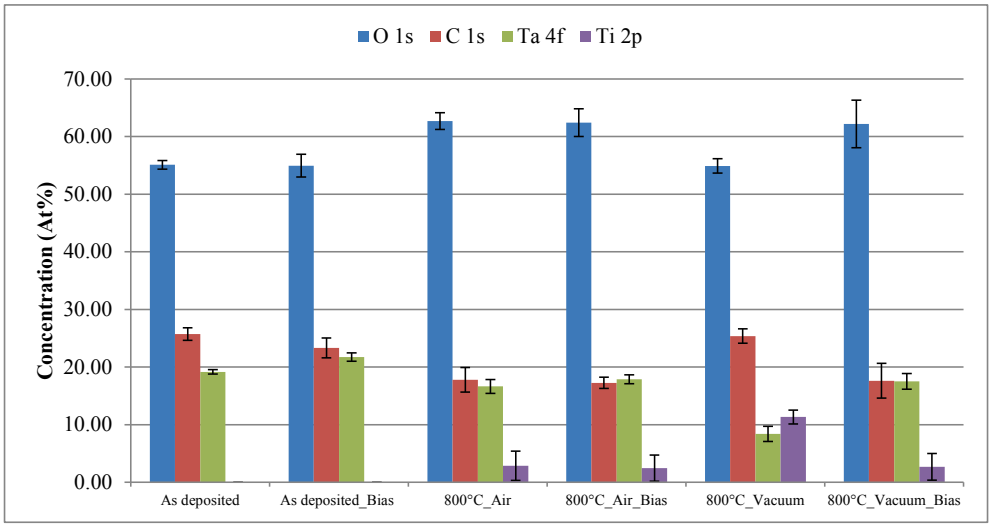

Fig. 4. Graph showing the average concentrations of oxygen, carbon, tantalum and titanium from XPS survey spectra on the surface of the unbiased and biased tantalum oxide films annealed in air and vacuum at 800 °C.

vacuum with a bias is approximately 7:1. The samples annealed in vacuum without a bias produce a less dense film which allows for Ti out-migration and cracking to occur. This explains why the Ti is higher in this ratio than the Ta. The application of a bias allows for a more-dense film which is less likely to crack and allow for Ti-out migration. From Fig. 4, the amount of Ti in as deposited film is marginal, but detectable from the presence of very weak Ti 2p peaks in the spectra. The amount of Ti rises at the surface of the annealed films, with vacuum annealing enhancing the amount but the application of a bias reducing the outmigration. The film deposited without any bias and then annealed at 800 °C in vacuum shows a significant presence of titanium (> 10 at.%) on the surface, indicating Ti migration through the tantalum oxide film. The application of a bias voltage can reduce the Ti-out migration.

High resolution XPS analysis show that O1s transition (Fig. 5(a)) for these films generally occurs between 530 and 530.5 eV, which is characteristic of higher oxide of tantalum, tantalum dioxide (TaO_2). The O1s peak appearing at 528 eV is also bonded to Ta but the lower binding energy of this peak indicates that this is a sub-oxide such as Ta_2O_3 or TaO, the oxidation state of which should be lower than the higher oxide [55]. The peaks appearing at 529 and 527 eV in Fig. 5a (iii) is associated with oxides of titanium. The O 1s peaks appearing at 532 eV are attributed to the oxygen-carbon bonds. We assigned the oxidation states of Ta by using the methodology developed in McNamara et al [55]. High resolution Ta 4f spectra (Fig. 5(b)) show that the main Ta peak appears at around 26 eV, which is characteristic of tantalum dioxide (TaO_2). Minor peaks appearing at 25 eV, 23.8 eV, 22.5 eV and 21 eV are characteristic of the sub-oxides Ta_2O_3, TaO, Ta_2O, and Ta metal respectively [55]. A 90:10 Ar to oxygen mixture results in a lower oxidation state of Ta which is mainly due to the low oxygen presence in the deposition chamber. The as-deposited films show the presence of a relatively small amount (1.5 at.% for as-deposited films and 0.7 at.% for films deposited with a bias) of sub-oxides present on the surface. Sub-oxides form as an intermediate before a stable oxide generally forms. Fig. 5(c) shows Ti 2p peak for the tantalum oxide film annealed in vacuum at 800 °C with no bias. This film showed the highest amount of Ti (Fig. 4) indicating clearly an out migration. Interestingly, the Ta 4f spectra for this sample (Fig. 5(b)) showed sub oxides in annealed samples which, from Fig. 4, have shown evidence of surface presence (within the XPS analysis depth of 3–10 nm). The peaks appearing 458, 457 and 456 eV are attributed to TiO_2, Ti_2O_3 and TiO respectively. As can be seen from Fig. 5(c) Ti ions have migrated to the surface of the sample. The presence of sub-oxides in annealed films indicate that Ti has reduced higher tantalum oxide to form titanium oxides by leaving Ta with its sub-oxides, in locations where Ta has lost oxygen to titanium, which would have a slightly higher affinity to oxygen than

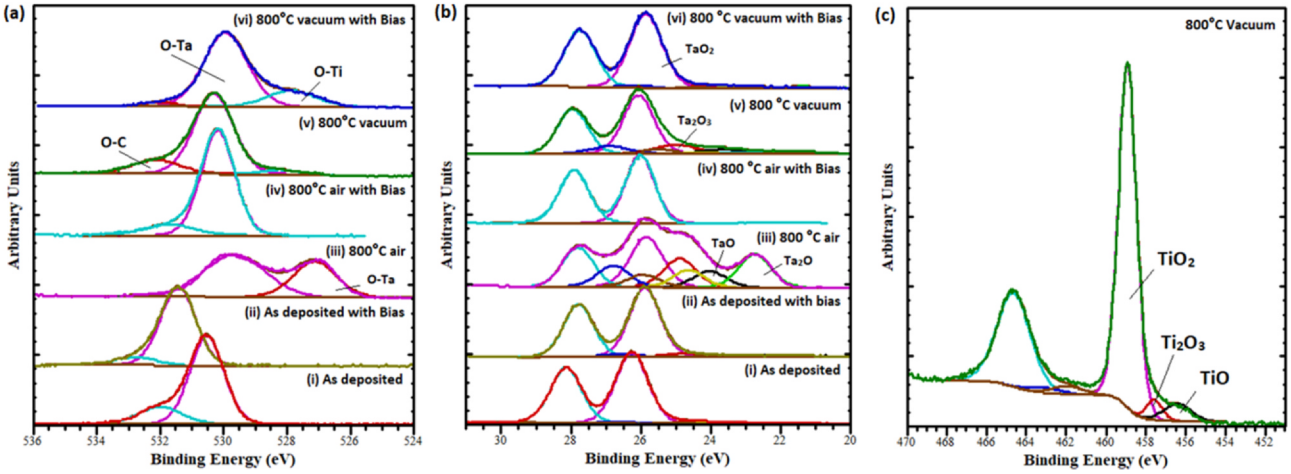

Fig. 5. XPS high resolution images of (a) O 1 s peaks, (b) Ta 4f peaks (c) Ti 2p peaks with (i) as deposited without a bias, (ii) as deposited with a bias, (iii) annealed at 800 °C in air without bias, (iv) annealed at 800 °C in air with bias, (v) annealed at 800 °C in vacuum without bias and (vi) annealed at 800 °C in vacuum with bias.

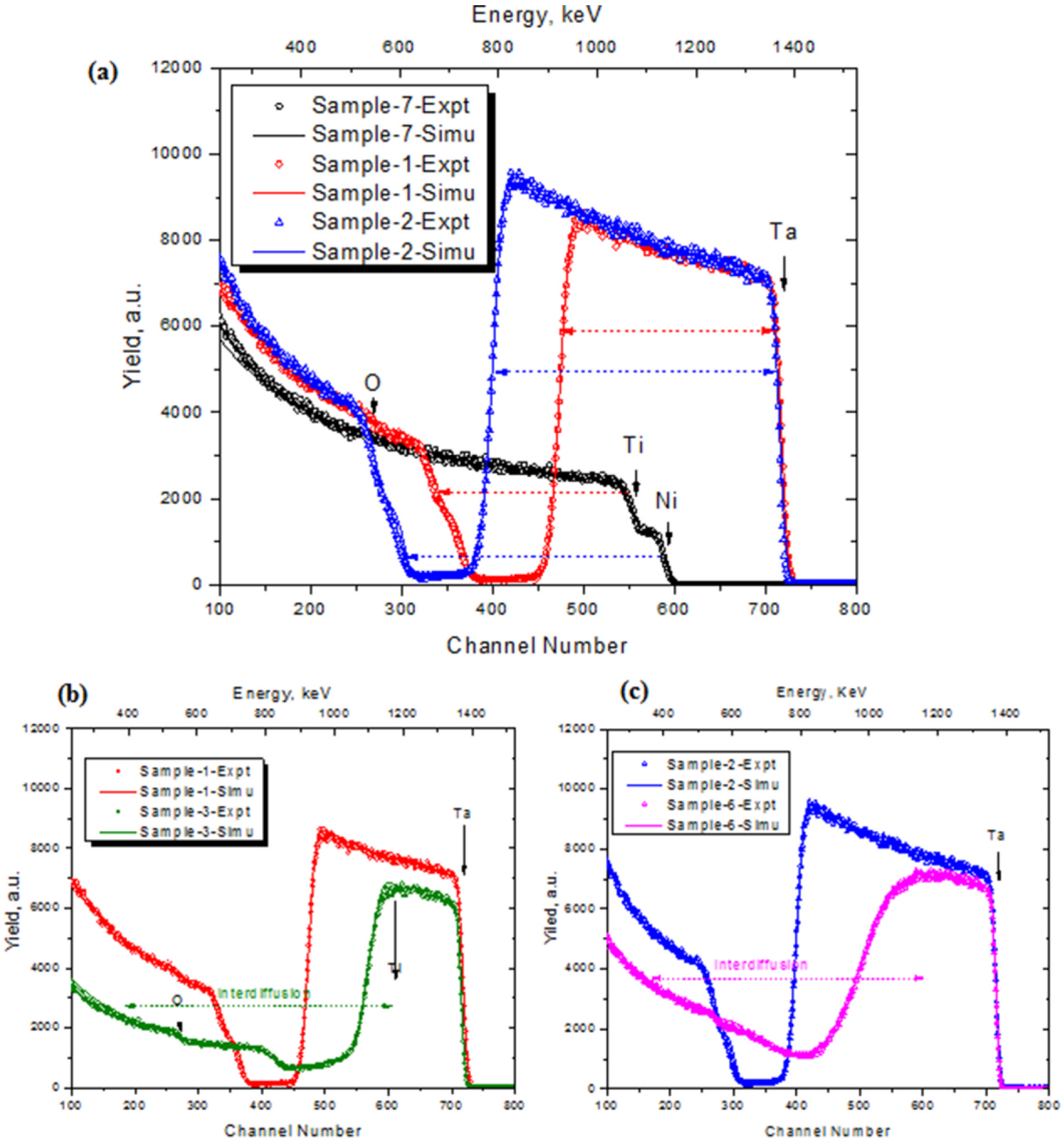

Fig. 6. (a) Sample-7: NiTi Substrates (Ti:Ni = 52:48); Sample-1: TaOx (30/70) as-sputtered (~460 nm); Sample-2: TaOx as-sputtered with Bias (~600 nm); (b) Sample-6: biased TaOx sample annealed at 800 °C in Vacuum; Ti, Ta, O interdiffusion; (c) Sample-3: TaOx sample Annealed at 800 °C in Air TaOx → Ta_2O_5.

tantalum.

Fig. 6 shows Rutherford backscattering spectrometry (RBS) of substrate materials, as deposited thin films and annealed samples. Standardised Ti thin film on vitreous carbon and computer-simulated spectra using SIMNRA software are used for elemental identification, film thickness and stoichiometry evaluation. Experimental and simulated RBS spectra are shown in Fig. 6(a–c), the leading edges of identifiable elements (O, Ti, Ni and Ta) are indicated with arrows. Energy loss or the shifting in backscatter energy is represented as thin film thickness and relative yield is a representation of relative atomic concentration of the individual elements. From Fig. 6(a), the energy spectra shifted as the TaOx thin films are grown on NiTi substrate (black line). The deposition with bias (Sample 2) resulted in a thicker TaOx film than sample 1 (no bias). From Fig. 6(a) it can be seen that both samples (1 and 2) have a similar TaOx stoichiometry. The relative yield of Ta/O peak represent a near identical stoichiometry of O:Ta = 30/70 for both Sample 1 and 2. Fig. 6(b) compares the as-deposited Ta-oxide films (Sample 1) and the Ta-oxide films annealed in air (Sample 3) and Fig. 6(c) compares the as-deposited Ta-oxide films with bias (Sample 2) and the Ta-oxide films annealed in vacuum with bias (Sample 6). It was found that as the samples are annealed at 800 °C in air and vacuum with bias, the relative stoichiometry of TaOx layers are different. With the presence of oxygen, the TaOx became Ta_2O_5 in the case of air-annealed film (sample 3). A slight reduction in relative yield of Ta is due to the Ti out diffusion. During the annealing process inter-diffusion resulted in a growing TaTiOx layer which buried the NiTi substrate and blocked the Ni out-diffusion. O in-diffusion, Ti out diffusion and burial of Ni are also revealed with characteristic X-ray spectra of $Ti_{K\alpha}$, $Ti_{K\beta}$, $Ni_{K\alpha}$, $Ni_{K\beta}$ and $Ta_{L\alpha}$ as shown in Fig. 7. Particle induced X-ray emission spectrometry (PIXE) spectra were taken on the samples simultaneously with RBS. The

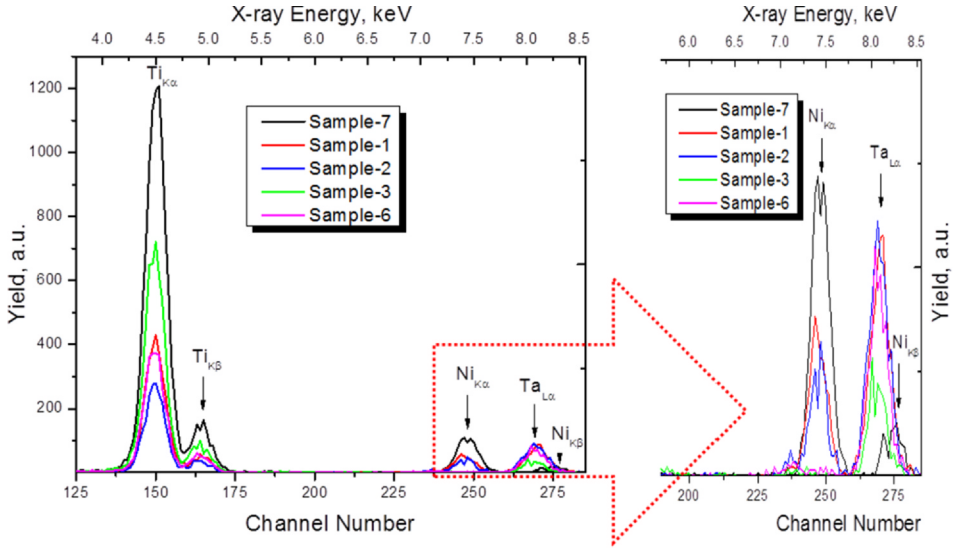

Fig. 7. PIXE spectra representing characteristic X-ray lines of Ti, Ni and Ta. Relative intensities are represented with higher yield. Ni and Ta peaks are magnified in the inset.

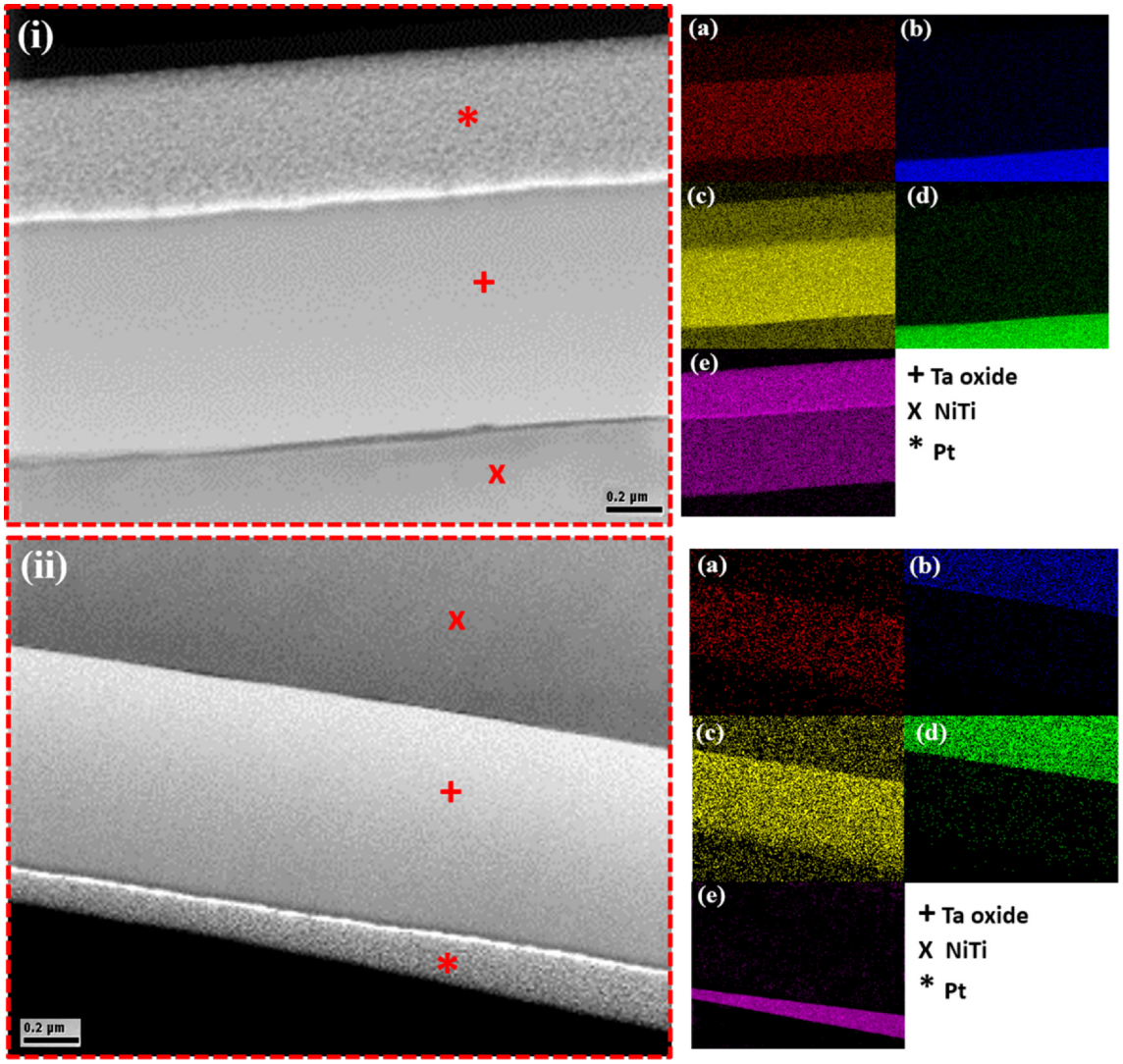

Fig. 8. Cross-sectional STEM micrographs of tantalum oxide films on NiTi substrates (i) as deposited without a bias and (ii) as deposited with a bias. The results from EDX mapping are also shown (a) oxygen, (b) nickel, (c) tantalum, (d) titanium and (e) platinum.

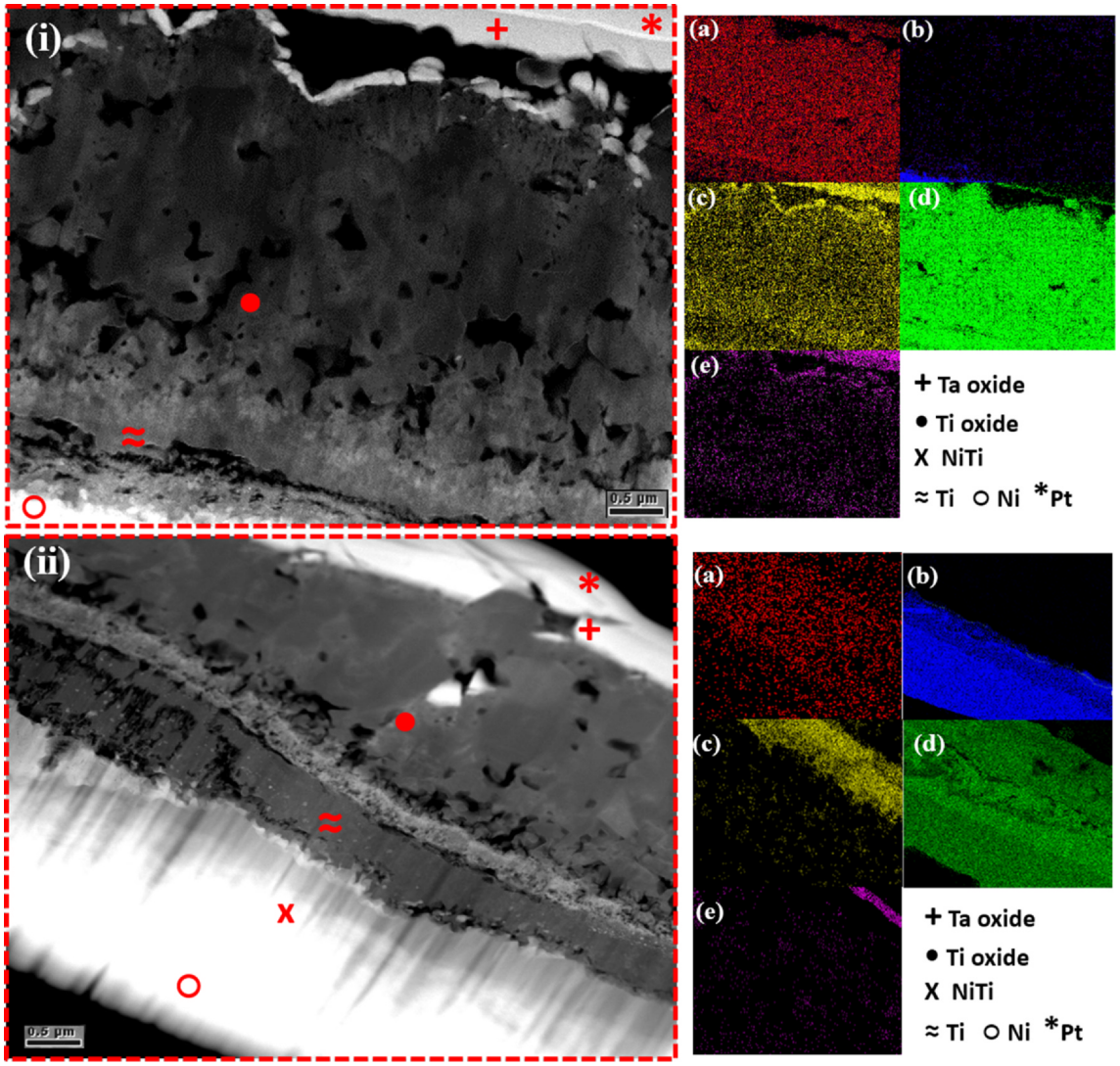

Fig. 9. Cross-sectional STEM micrographs of tantalum oxide films on NiTi substrates (i) annealed at 800 °C in air without bias and (ii) annealed at 800 °C in air with bias. The results from EDX mapping are also shown (a) oxygen, (b) nickel, (c) tantalum, (d) titanium and (e) platinum.

relative intensities of X-ray peaks represent relative abundance of elements visible to the incident ion beam. As the relative Ta-Ti-Ox layer grows with the in-diffusion of O and out diffusion of Ti, the NiTi substrate remains buried and Ni is blocked.

3.3. Interface analysis by cross sectional STEM

Transmission electron microscopy was used to investigate the microstructure of the tantalum oxide films deposited onto a NiTi substrate. Figs. 8–10 show STEM micrographs of tantalum oxide films deposited onto a NiTi substrate under different conditions. Fig. 8(i) shows as deposited tantalum oxide film and Fig. 8(ii) shows as deposited tantalum oxide film with a negative bias applied. As the films are amorphous, it was not possible to investigate the structure. EDX was used to identify the different layers present in the tantalum oxide films deposited onto NiTi. In the EDX map (a) oxygen, (b) nickel, (c) tantalum, (d) titanium and (e) platinum. The platinum layer was deposited onto all the samples to protect it from damage during the FIB preparation. From Fig. 8(i) it can be seen that there are three layers present in the sample. The EDX map shows that the films are composed of mainly platinum, tantalum oxide and NiTi. Fig. 8(ii) is similar to Fig. 8(i) in that there are three layers present in the sample mainly platinum, tantalum oxide and NiTi. The EDX map (e) is slightly different to the Figure (ii) here we suspect sample drift has occurred during the mapping process.

Fig. 9(i) shows the STEM image of the tantalum oxide film deposited on NiTi and annealed in air at 800 °C. From the image, it can be seen, that cracks are appearing in the Ta-oxide film. Annealing at 800 °C results in a porous TiO_2 layer [33]. When annealing in air more oxygen is present and therefore there is an increased oxygen migration into the tantalum oxide film which reacts with the TiO_2 layer already present to create a thicker TiO_2 layer. When the oxygen cannot react with the Ti in the TiO_2 layer anymore it pulls the Ti from the bulk NiTi which then leaves behind a nickel rich layer, as can be seen in the EDX map (a–e) for the sample. Fig. 9(ii) shows the micrograph of the tantalum oxide film deposited on NiTi with a −100 V bias and annealed in air at 800 °C. From Fig. 9(ii) it can be seen that the TiO_2 layer is migrating into the tantalum oxide film. It can be seen from the EDX map (a-e) that due to the inward migration of oxygen, the thickness of the TiO_2 layer has increased. The inward migration of oxygen results in the oxygen pulling titanium from the bulk. This results in a nickel rich layer developing, as can be seen from image (b) the EDX map. The contrast difference in the NiTi is a result of thinning of the substrate during sample preparation by FIB. The STEM results confirm the theory that was developed during SEM and XPS analysis that Ti ions are migrating to the surface. STEM results show that the application of a bias voltage

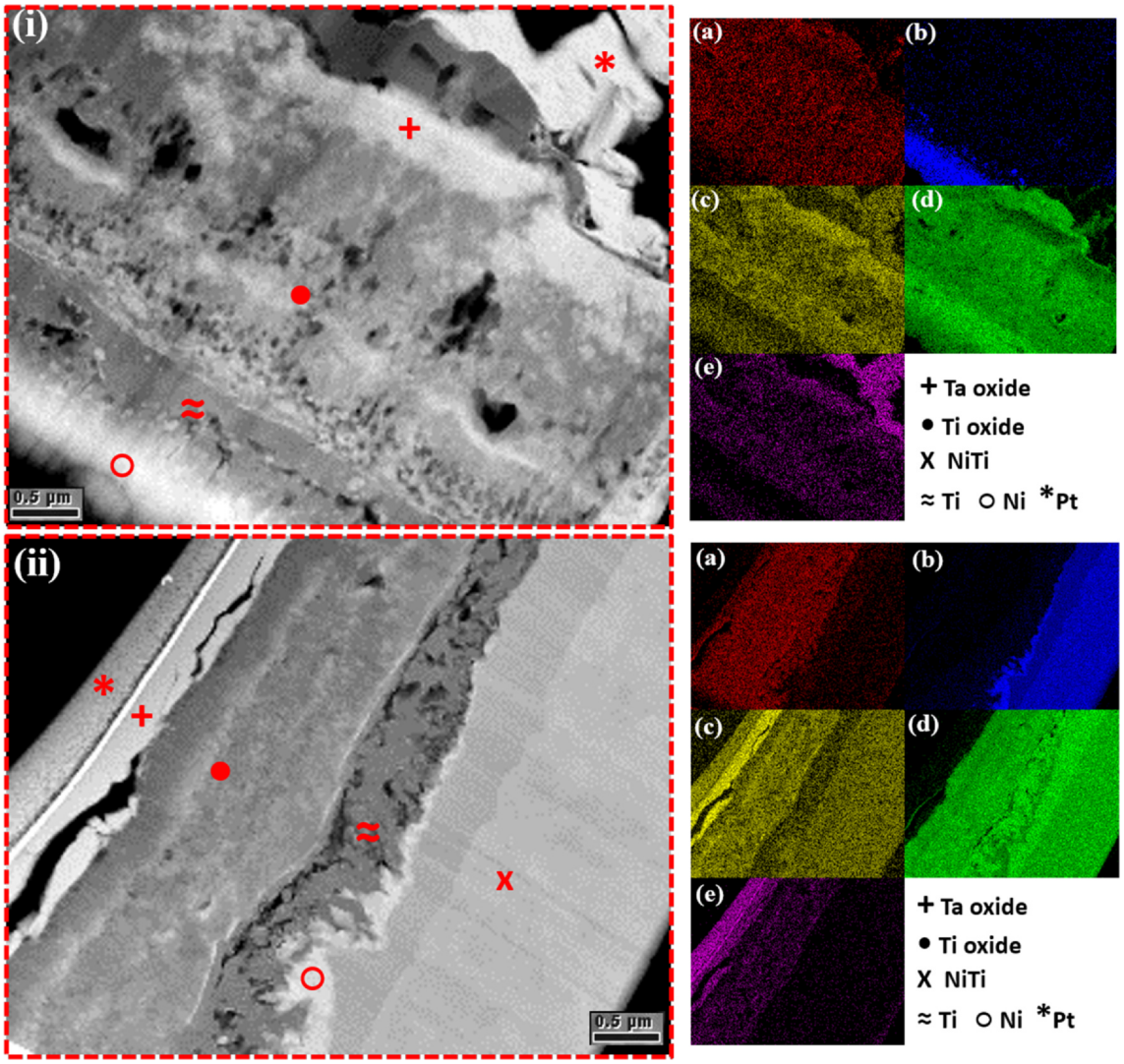

Fig. 10. Cross-sectional STEM micrographs of tantalum oxide films on NiTi substrates (i) annealed at 800 °C in vacuum without bias and (ii) annealed at 800 °C in vacuum with bias. The results from EDX mapping are also shown (a) oxygen, (b) nickel, (c) tantalum, (d) titanium and (e) platinum.

during deposition has helped preventing outward migration of Ti ions towards the tantalum oxide surface. As can be seen from the EDX map in Fig. 9(i) and (ii) that both Ta and Pt have diffused through the layers, this could be contributed to the porous nature of both the Ta-oxide and TiO_2 layers.

Fig. 10(i) shows a STEM micrograph of the tantalum oxide film deposited onto a NiTi substrate and annealed in vacuum at 800 °C. It can be seen, that titanium has migrated through the tantalum oxide film to the surface. The titanium dioxide layer is porous. According to Firstov et al [33], annealing at 800 °C can result in the growth of a porous TiO_2 layer. The higher annealing temperature has increased the oxygen migration into the tantalum oxide film and reacted with the TiO_2 layer already present to create a thicker TiO_2 layer. Titanium migration from the bulk NiTi results in a nickel rich layer. From Fig. 10(i), it can be seen that it is difficult to distinguish between the TiO_2 layer and the Ta-oxide layer. The EDX map shows the top-most layer to be platinum, it can also be seen that Ti has migrated to the surface and that the tantalum oxide film is beneath this layer. The EDX map shows that titanium dioxide is the next layer. Beneath this is a titanium layer, the outmigration of which has resulted in the formation of a nickel layer. Fig. 10(ii) shows a STEM micrograph of the tantalum oxide film deposited on NiTi with a −100 V bias and annealed in vacuum at 800 °C. Microcracks are visible in the Ta-oxide film. The higher annealing temperature has increased the oxygen migration into the tantalum oxide film and reacted with the TiO_2 layer already present to create a thicker TiO_2 layer. When the oxygen cannot react with the Ti in the TiO_2 layer anymore it pulls the Ti from the bulk NiTi which then leaves behind a nickel rich layer [18,19]. EDX map shows a nickel layer that has formed underneath the TiO_2 layer. Fig. 10(i) and (ii) thus show again that applying a negative bias helps preventing the out migration of TiO_2 into the tantalum oxide layer. The titanium dioxide layer in Fig. 10(ii) is not as porous as that in Fig. 10(i). The application of a bias resulted in a less porous film which makes Ti migration to the surface difficult. STEM results further confirm the observation made from SEM and XPS analyses that Ti ions do tend to out-migrate to the surface. Applying a bias during the deposition process helps prevent outward migration of Ti ions to the surface of the tantalum oxide film.

4. Conclusions

Annealing the tantalum oxide films on NiTi at 800 °C in both air and vacuum resulted in the outward migration of titanium ions to the surface. This can be seen from the XPS data where titanium is detected within the first 10 nm. It was established that the tantalum films deposited without a bias voltage results in a less dense film through which an inward migration of oxygen and outward migration of titanium is

easier. In order to address this issue a negative bias of −100 V was applied to the substrate during the deposition process. It was found that while outward migration of titanium had occurred the concentration of Ti was less than that in the samples deposited without a bias. A higher bias may help further prevention of Ti-outmigration.

We have found that a thin layer of reactively sputtered tantalum (Ta) oxide on the bulk NiTi restricts Ti-out-migration and creates a biocompatible Ti/Ta interdiffusion layer that provides a larger barrier against Ni leaching and potentially improve long-term biocompatibility of NiTi.

CRediT authorship contribution statement

K. McNamara: Conceptualization, Methodology, Formal analysis, Investigation, Resources, Writing - original draft, Visualization. **S. Belochapkine:** Investigation. **K.M. Hossain:** Investigation, Visualization. **M.S. Dhoubhadel:** Investigation. **S.A.M Tofail:** Conceptualization, Writing - review & editing, Supervision.

Declaration of Competing Interest

The authors declare that they have no known competing financial interests or personal relationships that could have appeared to influence the work reported in this paper.

Appendix A. Supplementary material

Supplementary data to this article can be found online at https://doi.org/10.1016/j.apsusc.2020.147621.

References

[1] W.J. Buehler, F.E. Wang, A summary of recent research on the Nitinol alloys and their potential application in ocean engineering, Ocean Eng. 1 (1968) 105–120, https://doi.org/10.1016/0029-8018(68)90019-X.

[2] T. Duerig, A. Pelton, D. Stockel, An overview of nitinol medical applications, Mater. Sci. Eng. A. 149 (1999) 273–275, https://doi.org/10.1016/S0921-5093(99)00294-4.

[3] K. Otsuka, C.M. Wayman, Shape Memory Materials, Cambridge University Press, Cambridge, 1999.

[4] K. Otsuka, X. Ren, Physical metallurgy of Ti–Ni-based shape memory alloys, Prog. Mater. Sci. 50 (5) (2005) 511–678, https://doi.org/10.1016/j.pmatsci.2004.10.001.

[5] A. Biscarini, G. Mazzolai, A. Tuissi, Enhanced nitinol properties for biomedical applications, Recent Pat. Biomed. Eng. 1 (2008) 180–196, https://doi.org/10.2174/1874764710801030180.

[6] D. Mantovani, Shape memory alloys: properties and biomedical applications, JOM 52 (2000) 36–44, https://doi.org/10.1007/s11837-000-0082-4.

[7] N.B. Morgan, Medical shape memory alloy applications—the market and its products, Mater. Sci. Eng. A. 378 (2004) 16–23, https://doi.org/10.1016/j.msea.2003.10.326.

[8] C. Trepanier, R. Venugopalan, A.R. Pelton, Corrosion resistance and biocompatibility of passivated NiTi, in: L. Yahia (Ed.), Shape Memory Implants, Springer, Berlin, 2000, pp. 35–45.

[9] H. Tian, D. Schryvers, S. Shabalovskaya, J. Van Humbeeck, Microstructure of surface and subsurface layers of a Ni-Ti shape memory microwire, Microsc. Microanal. 15 (1) (2009).

[10] S. Shabalovskaya, J. Anderegg, J. Van Humbeeck, Critical overview of Nitinol surfaces and their modifications for medical applications, Acta Biomater. 4 (2008) 447–467, https://doi.org/10.1016/j.actbio.2008.01.013.

[11] S.A. Shabalovskaya, Surface, corrosion and biocompatibility aspects of Nitinol as an implant material, Bio-Med. Mater. Eng. 12 (2002) 69–109.

[12] D.J. Wever, A.G. Veldhuizen, J. De Vries, H.J. Busscher, D.R.A. Uges, J.R. Van Horn, Electrochemical and surface characterization of a nickel–titanium alloy, Biomaterials. 19 (7–9) (1998) 761–769, https://doi.org/10.1016/S0142-9612(97)00210-X.

[13] D.J. Wever, A.G. Veldhuizen, M.M. Sanders, J.M. Schakenraad, J.R. Van Horn, Cytotoxic, allergic and genotoxic activity of a nickel-titanium alloy, Biomaterials. 18 (16) (1997) 1115–1120, https://doi.org/10.1016/S0142-9612(97)00041-0.

[14] J. Ryhänen, Biocompatibility of nitinol, Minim. Invasive Ther. Allied Technol. 9 (2) (2000) 99–105, https://doi.org/10.3109/13645700009063056.

[15] S. Shabalovskaya, J. Van Humbeeck, Biocompatibility of nitinol for biomedical applications, in: T. Yoneyama, S. Miyazaki (Eds.), Shape Memory Alloys for Biomedical Applications, Woodhead Pub, Cambridge, 2008, pp. 194–236.

[16] S. Nagaraja, S.J. Sullivan, P.R. Stafford, A.D. Lucas, E. Malkin, Impact of nitinol stent surface processing on in-vivo nickel release and biological response, Acta Biomater. 72 (2018) 424–433, https://doi.org/10.1016/j.actbio.2018.03.036.

[17] J. Ševčíková, D. Bártková, M. Goldbergová, M. Kuběnová, J. Čermák, J. Frenzel, A. Weiser, A. Dlouhý, On the Ni-Ion release rate from surfaces of binary NiTi shape memory alloys, Appl. Surf. Sci. 427 (2018) 434–443, https://doi.org/10.1016/j.apsusc.2017.08.235.

[18] M. Nolan, S.A.M. Tofail, Density functional theory simulation of titanium migration and reaction with oxygen in the early stages of oxidation of equiatomic NiTi alloy, Biomaterials 31 (13) (2010) 3439–3448, https://doi.org/10.1016/j.biomaterials.2010.01.060.

[19] M. Nolan, S.A.M. Tofail, The atomic level structure of the TiO_2-NiTi interface, Phys. Chem. Chem. Phys. 12 (33) (2010) 9742–9750, https://doi.org/10.1039/C002562C.

[20] B. Feng, J. Weng, B. Yang, J. Chen, J. Zhao, L. He, S. Qi, X. Zhang, Surface characterization of titanium and adsorption of bovine serum albumin, Mater. Charact. 49 (2) (2002) 129–137, https://doi.org/10.1016/S1044-5803(02)00341-8.

[21] S.A. Shabalovskaya, H. Tian, J.W. Anderegg, D.U. Schryvers, W.U. Carroll, J. Van Humbeeck, The influence of surface oxides on the distribution and release of nickel from Nitinol wires, Biomaterials 30 (4) (2009) 468–477, https://doi.org/10.1016/j.biomaterials.2008.10.014.

[22] W. Carroll, M. Kelly, Corrosion behavior of Nitinol wires in body fluid environment, J. Biomed. Mater. Res. 67A (2003) 1123–1130, https://doi.org/10.1002/jbm.a.10099.

[23] S.A. Shabalovskaya, Biological aspects of TiNi alloy surfaces, J. Phys. IV. 5 (1995) 1199–1204, https://doi.org/10.1051/jp4/1995581199.

[24] B. Thierry, M. Tabrizian, C. Trepanier, O. Savadogo, L.H. Yahia, Effect of surface treatment and sterilization processes on the corrosion behavior of NiTi shape memory alloy, J. Biomed. Mater. Res. 51 (4) (2000) 685–693, https://doi.org/10.1002/1097-4636(20000915)51:4<685::AID-JBM17>3.0.CO;2-S.

[25] R. Venugopalan, C. Trepanier, Assessing the corrosion behaviour of Nitinol for minimally-invasive device design, Minim. Invasive Ther. Allied Technol. 9 (2) (2000) 67–73, https://doi.org/10.3109/13645700009063052.

[26] C. Huang, Y. Xie, L. Zhou, H. Huang, Enhanced surface roughness and corrosion resistance of NiTi alloy by anodization in diluted HF solution, Smart Mater. Struct. 18 (2) (2009) 024003, , https://doi.org/10.1088/0964-1726/18/2/024003.

[27] Z. Yang, X. Wei, W. Gao, P. Cao, Anodization of NiTi alloy in an ethylene glycol electrolyte, Surf. Coat. Technol. 252 (2014) 142–147, https://doi.org/10.1016/j.surfcoat.2014.04.060.

[28] M. Chembath, J.N. Balaraju, M. Sujata, Effect of anodization and annealing on corrosion and biocompatibility of NiTi alloy, Surf. Coat. Technol. 302 (2016) 302–309, https://doi.org/10.1016/j.surfcoat.2016.06.031.

[29] M. Saugo, D.O. Flamini, G. Zampieri, S.B. Saidman, Corrosion resistance improvement of nitinol by anodisation in the presence of molybdate ions, Mater. Chem. Phys. 190 (2017) 136–145, https://doi.org/10.1016/j.matchemphys.2017.01.017.

[30] N. Ohtsu, Y. Hirano, K. Takiguchi, Comparison of NiTi alloy surfaces formed by anodization in nitric, phosphoric, and sulfuric acid electrolytes, Surf. Coat. Tech. 335 (2018), https://doi.org/10.1016/j.surfcoat.2017.12.050.

[31] N. Ohtsu, Y. Hirano, Growth of oxide layers on NiTi alloy surfaces through anodization in nitric acid electrolyte, Surf. Coat. Tech. 325 (2017) 75–80, https://doi.org/10.1016/j.surfcoat.2017.06.021.

[32] C. Trepanier, M. Tabrizian, L.H. Yahia, L. Bilodeau, D.L. Piron, Effect of modification of oxide layer on NiTi stent corrosion resistance, J. Biomed Mater. Res., Part A 43 (4) (1998) 433–440, https://doi.org/10.1002/(SICI)1097-4636(199824)43:4<433::AID-JBM11>3.0.CO;2-%23.

[33] G.S. Firstov, R.G. Vitchev, H. Kumar, B. Blanpain, J. Van Humbeeck, Surface oxidation of NiTi shape memory alloy, Biomaterials 23 (24) (2002) 4863–4871, https://doi.org/10.1016/S0142-9612(02)00244-2.

[34] D. Vojtěch, M. Voděrová, J. Fojt, P. Novák, T. Kubásek, Surface structure and corrosion resistance of short-time heat-treated NiTi shape memory alloy, Appl. Surf. Sci. 257 (5) (2010) 1573–1582, https://doi.org/10.1016/j.apsusc.2010.08.097.

[35] J. Wang, B.X.T. Wang, Effects of high temperature oxidation on the structure and properties of NiTi alloy, Asian J. Chem. 24 (9) (2012) 3936–3938.

[36] Z. Wu, A. Mahmud, J. Zhang, Y. Liu, H. Yang, Surface oxidation of NiTi during thermal exposure in flowing argon environment, Mater. Des. 140 (2018) 123–133, https://doi.org/10.1016/j.matdes.2017.11.061.

[37] A. Mahmud, Z. Wu, J. Zhang, Y. Liu, H. Yang, Surface oxidation of NiTi and its effects on thermal and mechanical properties, Intermetallics 103 (2018) 52–62, https://doi.org/10.1016/j.intermet.2018.09.013.

[38] J. Kim, J.K. Park, H.K. Kim, A.R. Unnithan, C.S. Kim, C.H. Park, Optimization of electropolishing on NiTi alloy stents and its influence on corrosion behavior, J. Nanosci. Nanotechnol. 17 (4) (2017) 2333–2339, https://doi.org/10.1166/jnn.2017.13324.

[39] S. Jin, Y. Zhang, Q. Wang, D. Zhang, S. Zhang, Influence of TiN coating on the biocompatibility of medical NiTi alloy, Colloids Surf. B. 101 (2013) 343–349, https://doi.org/10.1016/j.colsurfb.2012.06.029.

[40] A. Shanaghi, P.K. Chu, A.R.S. Rouhaghdam, R. Xu, T. Hu, Structure and corrosion resistance of Ti/TiC coatings fabricated by plasma immersion ion implantation and deposition on nickel–titanium, Surf. Coat. Technol. 229 (2013) 151–155, https://doi.org/10.1016/j.surfcoat.2012.07.063.

[41] H. Maleki-Ghaleh, J. Khalil-Allafi, V. Khalili, M.S. Shakeri, M. Javidi, Effect of hydroxyapatite coating fabricated by electrophoretic deposition method on corrosion behavior and nickel release of NiTi shape memory alloy, Mater. Corros. 65 (7) (2014) 725–732, https://doi.org/10.1002/maco.201206950.

[42] S. Yang, F. Zhou, T. Xiao, D. Xu, Z. Li, Z. Xiao, Z.A. Xiao, Surface modification with SiO_2 coating on biomedical TiNi shape memory alloy by sol–gel method, Trans. Nonferrous Met. Soc. China 25 (11) (2015) 3723–3728, https://doi.org/10.1016/

S1003-6326(15)64015-8.
[43] K. Dudek, T. Goryczka, Electrophoretic deposition and characterization of thin hydroxyapatite coatings formed on the surface of NiTi shape memory alloy, Ceram. Int. 42 (16) (2016) 19124–19132, https://doi.org/10.1016/j.ceramint.2016.09.074.
[44] L. Zhang, Y. Duan, Z. Gao, J. Ma, R. Liu, S. Liu, Z. Tu, Y. Liu, C. Bai, L. Cui, F. Yang, Graphene enhanced anti-corrosion and biocompatibility of NiTi alloy, NanoImpact. 7 (2017) 7–14, https://doi.org/10.1016/j.impact.2016.10.003.
[45] N.I.A. Lopes, N.H.J. Freire, P.D. Resende, L.A. Santos, V.T.L. Buono, Electrochemical deposition and characterization of ZrO2 ceramic nanocoatings on superelastic NiTi alloy, Appl. Surf. Sci. 450 (2018) 21–30, https://doi.org/10.1016/j.apsusc.2018.04.154.
[46] F. Marashi-Najafi, J. Khalil-Allafi, M.R. Etminanfar, Biocompatibility of hydroxyapatite coatings deposited by pulse electrodeposition technique on the Nitinol superelastic alloy, Mater. Sci. Eng. C 76 (2017) 278–286, https://doi.org/10.1016/j.msec.2017.03.064.
[47] D. Vokoun, J. Racek, L. Kadeřávek, C.C. Kei, Y.S. Yu, L. Klimša, P. Šittner, Atomic layer-deposited TiO_2 coatings on NiTi surface, J. Mater. Eng. Perform. 27 (2) (2018).
[48] G.L. Burke, The corrosion of metals in tissues; and an introduction to tantalum, Can. Med. Assoc. J. 43 (2) (1940) 125–128.
[49] J. Black, Biologic performance of tantalum, Clin. Mater. 16 (3) (1994) 167–173, https://doi.org/10.1016/0267-6605(94)90113-9.
[50] Y.X. Leng, J.Y. Chen, P. Yang, H. Sun, J. Wang, N. Huang, The biocompatibility of the tantalum and tantalum oxide films synthesized by pulse metal vacuum arc source deposition, Nucl. Instrum. Methods Phys. Res., Sect. B. 242 (1–2) (2006) 30–32, https://doi.org/10.1016/j.nimb.2005.08.002.
[51] H. Moreira, A. Costa-Barbosa, S.M. Marques, P. Sampaio, S. Carvalho, Evaluation of cell activation promoted by tantalum and tantalum oxide coatings deposited by reactive DC magnetron sputtering, Surf. Coat. Tech. 330 (2017) 260–269, https://doi.org/10.1016/j.surfcoat.2017.10.019.
[52] C. Park, S. Kim, H.E. Kim, T.S. Jang, Mechanically stable tantalum coating on a nano-roughened NiTi stent for enhanced radiopacity and biocompatibility, Surf. Coat. Technol. 305 (2016) 139–145, https://doi.org/10.1016/j.surfcoat.2016.08.014.
[53] K. McNamara, O. Kolaj-Robin, S. Belochapkine, F. Laffir, A.A. Gandhi, S.A.M. Tofail, Surface chemistry and cytotoxicity of reactively sputtered tantalum oxide films on NiTi plates, Thin Solid Films. 589 (2015) 1–7, https://doi.org/10.1016/j.tsf.2015.04.070.
[54] Y. Zhou, M. Li, Y. Cheng, Y.F. Zheng, T.F. Xi, S.C. Wei, Tantalum coated NiTi alloy by PIIID for biomedical application, Surf. Coat. Technol. 228 (2013) S2–S6, https://doi.org/10.1016/j.surfcoat.2012.11.002.
[55] K. McNamara, S.A.M. Tofail, D. Conroy, J. Butler, A.A. Gandhi, W. Redington, X-ray analyses of thermally grown and reactively sputtered oxide films on NiTi alloy, Nucl. Instrum. Methods Phys. Res., Sect. B. (2012) 49–52, https://doi.org/10.1016/j.nimb.2011.07.106.
[56] S.J.J. Wu, B. Houng, B.S. Huang, Effect of growth and annealing temperatures on crystallization of tantalum pentoxide thin film prepared by RF magnetron sputtering method, J. Alloys Compd. 475 (1–2) (2009) 488–493, https://doi.org/10.1016/j.jallcom.2008.07.126.
[57] S. Jagadeesh Chandra, C.J. Choi, S. Uthanna, G. Mohan Rao, Structural and electrical properties of radio frequency magnetron sputtered tantalum oxide films: influence of post-deposition annealing, Mater. Sci. Semicond. Process. 13 (4) (2010) 245–251, https://doi.org/10.1016/j.mssp.2010.08.002.
[58] A. Ispas, B. Adolphi, A. Bund, F. Endres, On the electrodeposition of tantalum from three different ionic liquids with the bis (trifluoromethyl sulfonyl) amide anion, Phys. Chem. Chem. Phys. 12 (8) (2010) 1793–1803, https://doi.org/10.1039/B922071M.
[59] Y.M. Zhou, Z. Xie, H.N. Xiao, P.F. Hu, J. He, Effects of deposition parameters on tantalum films deposited by direct current magnetron sputtering in Ar–O_2 mixture, Appl. Surf. Sci. 258 (5) (2011) 1699–1703, https://doi.org/10.1016/j.apsusc.2011.10.012.
[60] A.X. Wei, Z.X. Ge, X.H. Zhao, J. Liu, Y. Zhao, Electrical and optical properties of tantalum oxide thin films prepared by reactive magnetron sputtering, J. Alloys Compd. 509 (41) (2011) 9758–9763, https://doi.org/10.1016/j.jallcom.2011.08.019.
[61] F. Meng, Z. Li, X. Liu, Synthesis of tantalum thin films on titanium by plasma immersion ion implantation and deposition, Surf. Coat. Technol. 229 (2013) 205–209, https://doi.org/10.1016/j.surfcoat.2012.04.044.
[62] M.S. Farhan, E. Zalnezhad, A.R. Bushroa, Properties of Ta_2O_5 thin films prepared by ion-assisted deposition, Mater. Res. Bull. 48 (10) (2013) 4206–4209, https://doi.org/10.1016/j.materresbull.2013.06.068.
[63] V.A. Luzanov, A.S. Vedeneev, V.V. Ryl'kov, M.P. Temiryazeva, A.M. Kozlov, M.P. Dukhnovskii, A.S. Bugaev, Synthesis of thin tantalum films by magnetron sputtering, J. Commun. Technol. Electron. 60 (12) (2015) 1325–1327, https://doi.org/10.1134/S1064226915110133.
[64] X. Yu, L. Tan, H. Yang, K. Yang, Surface characterization and preparation of Ta coating on Ti6Al4V alloy, J. Alloys Compd. 644 (2015) 698–703, https://doi.org/10.1016/j.jallcom.2015.04.207.
[65] B. Rahmati, A.A. Sarhan, W.J. Basirun, W.A.B.W. Abas, Ceramic tantalum oxide thin film coating to enhance the corrosion and wear characteristics of Ti6Al4V alloy, J. Alloys Compd. 676 (2016) 369–376, https://doi.org/10.1016/j.jallcom.2016.03.188.
[66] B. Rahmati, A.A. Sarhan, E. Zalnezhad, Z. Kamiab, A. Dabbagh, D. Choudhury, W.A.B.W. Abas, Development of tantalum oxide (Ta-O) thin film coating on biomedical Ti-6Al-4V alloy to enhance mechanical properties and biocompatibility, Ceram. Int. 42 (1) (2016) 466–480, https://doi.org/10.1016/j.ceramint.2015.08.133.
[67] T. Henke, M. Knaut, M. Geidel, F. Winkler, M. Albert, J.W. Bartha, Atomic layer deposition of tantalum oxide thin films using the precursor tert-butylimido-tris-ethylmethylamido-tantalum and water: process characteristics and film properties, Thin Solid Films 627 (2017) 94–105, https://doi.org/10.1016/j.tsf.2017.02.047.
[68] I. Perez, J.L.E. Carrejo, V. Sosa, F.G. Perera, J.R.F. Mancillas, J.T.E. Galindo, C.I.R. Rodríguez, Evidence for structural transition in crystalline tantalum pentoxide films grown by RF magnetron sputtering, J. Alloys Compd. 712 (2017) 303–310, https://doi.org/10.1016/j.jallcom.2017.04.073.
[69] H. Ghorbani, A. Abdollah-Zadeh, F. Bagheri, A. Poladi, Improving the bio-corrosion behavior of AISI316L stainless steel through deposition of Ta-based thin films using PACVD, Appl. Surf. Sci. 456 (2018), https://doi.org/10.1016/j.apsusc.2018.06.154.
[70] S. Shiri, A. Odeshi, N. Chen, R. Feng, R. Sutarto, Q. Yang, FCC tantalum thin films deposited by magnetron sputtering, Surf. Coat. Tech. 358 (2019) 942–946.
[71] Y. Li, S. Sanna, K. Norrman, D.V. Christensen, C.S. Pedersen, J.M.G. Lastra, M.L. Traulsen, V. Esposito, N. Pryds, Tuning the stoichiometry and electrical properties of tantalum oxide thin films, Appl. Surf. Sci. 470 (2019) 1071–1074, https://doi.org/10.1016/j.apsusc.2018.11.153.
[72] A.C. Hee, Y. Zhao, S.S. Jamali, P.J. Martin, A. Bendavid, H. Peng, X. Cheng, Corrosion behaviour and microstructure of tantalum film on Ti6Al4V substrate by filtered cathodic vacuum arc deposition, Thin Solid Films 636 (2017) 54–62, https://doi.org/10.1016/j.tsf.2017.05.030.
[73] Y. Cheng, W. Cai, H.T. Li, Y.F. Zheng, Surface modification of NiTi alloy with tantalum to improve its biocompatibility and radiopacity, J. Mater. Sci 41 (15) (2006) 4961–4964, https://doi.org/10.1007/s10853-006-0096-6.
[74] Y. Li, S. Wei, X. Cheng, T. Zhang, G. Cheng, Corrosion behavior and surface characterization of tantalum implanted TiNi alloy, Surf. Coat. Technol. 202 (13) (2008) 3017–3022, https://doi.org/10.1016/j.surfcoat.2007.11.003.
[75] A.W. Hassel, L. Neelakantan, A. Zelenkevych, A. Ruh, M. Spiegel, Selective de-alloying of NiTi by oxochloridation, Corros. Sci. 50 (5) (2008) 1368–1375, https://doi.org/10.1016/j.corsci.2008.01.022.
[76] A.I. Mardare, A. Savan, A. Ludwig, A.D. Wieck, A.W. Hassel, A combinatorial passivation study of Ta–Ti alloys, Corros. Sci. 51 (7) (2009) 1519–1527, https://doi.org/10.1016/j.corsci.2008.12.003.
[77] R.J. Hanrahan, D.P. Butt, Oxidation kinetics and mechanisms of Ti-Ta alloys, Oxid. Met. 47 (3) (1997) 317–353, https://doi.org/10.1007/BF01668517.
[78] M. Ohring, The Materials Science of Thin Films, second ed., Academic Press, San Diego, 1992.